Role of Delays in Shaping Spatiotemporal Dynamics of Neuronal Activity in Large Networks

Alex Roxin, Nicolas Brunel, and David Hansel

Laboratory of Neurophysics and Physiology, UMR8119 CNRS - Université René Descartes, 45 Rue des Saints Pères, 75270 Paris Cedex 06, France

(Received 15 October 2004; published 16 June 2005)

We study the effect of delays on the dynamics of large networks of neurons. We show that delays give rise to a wealth of bifurcations and to a rich phase diagram, which includes oscillatory bumps, traveling waves, lurching waves, standing waves arising via a period-doubling bifurcation, aperiodic regimes, and regimes of multistability. We study the existence and the stability of the various dynamical patterns analytically and numerically in a simplified rate model as a function of the interaction parameters. The results derived in that framework allow us to understand the origin of the diversity of dynamical states observed in large networks of spiking neurons.

DOI: 10.1103/PhysRevLett.94.238103 PACS numbers: 87.19.La, 05.45.Jn, 84.35.+i, 89.75.Hc

Electrophysiological and anatomical data indicate that the cerebral cortex is spatially and functionally organized [1–3]. These patterns of connectivity must influence the intrinsic dynamics of cortical circuits which can now be visualized using optical techniques [4]. The relationship between the spatial profile of neural interactions and spatio-temporal patterns of neuronal activity can be investigated in modeling studies. It has been shown that localized bumps of neuronal activity emerge in neural circuits with translationally invariant local excitation combined with global inhibition. It has been proposed that orientation selectivity in V1 is a functional counterpart of such patterns [5–7]. It has been suggested that localized bumps arising via a subcritical bifurcation may underlie spatial short-term memory [8,9]. Traveling waves and localized traveling bumps may also arise depending on connectivity and on the neuronal and synaptic dynamics [6,10,11].

An important property of neural interactions is that they involve delays. Delays, on the order of milliseconds, are due to the finite-velocity propagation of action potentials as well as to both dendritic and synaptic processing [12]. Effective delays can also be induced by the spike-generation dynamics [13]. It has been shown elsewhere that such delays may lead to homogeneous oscillations in inhibitory networks with homogeneous, random connectivity [14,15]. In this Letter we show that when interactions are spatially structured, delays induce a wealth of dynamical states with different spatio-temporal properties and domains of multistability.

Insight into the dynamics of cortical tissue can be gained using firing-rate models [5,6,16–19]. Most previous studies of firing-rate models have not considered the specific effects of delays. In the first part of this work we consider the following equation

$$\tau \dot{m} = -m + \Phi\left[I(x) + \int dy J(|x-y|) m(y, t-D) \right], \quad (1)$$

where $m(x)$ is the activity of neurons at a 1D location on a periodic ring $x \in [-\pi, \pi]$, τ is the time constant of rate dynamics (in the following, we take $\tau = 1$ without loss of generality), and Φ is the steady-state current-to-rate transfer function. For simplicity, we assume that $\Phi(I)$ is threshold linear, $\Phi(I) = I$ if $I > 0$, and $\Phi(I) = 0$ otherwise. The total synaptic input is split into an external current $I(x)$ and the synaptic current due to the presynaptic activity at a location y with a weight $J(|x-y|)$ and a delay D.

In the absence of delay (i.e., $D = 0$), the dynamics of Eq. (1) for a stationary, homogeneous external input converge to a stable fixed point for which the activity of the neurons is either homogeneous or localized, depending on the spatial modulation of the interactions [5,6].

Here we consider the case of $D > 0$. In this case the stability of the stationary uniform state with respect to perturbations of wave number n is given by the dispersion relation $\lambda = -1 + J_n e^{-\lambda D}$, where $J_n = \frac{1}{2\pi} \int_{-\pi}^{\pi} dy J(y) \times \cos ny$. A steady instability of the nth mode occurs for $J_n = 1$ while for $J_n \cos(D\omega) = 1$ there is an oscillatory instability with frequency $\omega = -\tan(D\omega)$. Hence, four types of linear instability of the stationary uniform state are possible, including: (i) a firing-rate instability ($\omega = 0$, $n = 0$), (ii) a Hopf instability ($\omega \neq 0, n = 0$), (iii) a Turing instability ($\omega = 0$, $n \neq 0$), and (iv) a Turing-Hopf instability ($\omega \neq 0$, $n \neq 0$). In the following we study the characteristics and stability of the nonlinear firing patterns arising from these instabilities. We assume for simplicity that the interaction has only two nonzero Fourier components: $J(|x-y|) = J_0 + J_1 \cos(x-y)$. For $J_0 > |J_1|$, the interaction is purely excitatory, while for $J_0 < -|J_1|$ it is purely inhibitory. For $J_1 > |J_0|$ the connectivity is locally excitatory and inhibitory at larger distances, (Mexican hat), while for $J_1 < -|J_0|$ the inverse is true.

Analytical and numerical investigation of Eq. (1) reveals a phase diagram in the J_0, J_1 plane, Fig. 1, in which one can discern eight states of activity: stationary uniform (SU), stationary bump (SB), oscillatory bump (OB), oscillatory uniform (OU), traveling waves (TW), standing waves (SW), lurching waves (LW) and aperiodic dynamics (A). In the following we discuss the three nonlinear solutions (SB, OU, TW) which arise via primary bifurcations of the SU state, and whose stability can be solved analytically

 © 2005 The American Physical Society

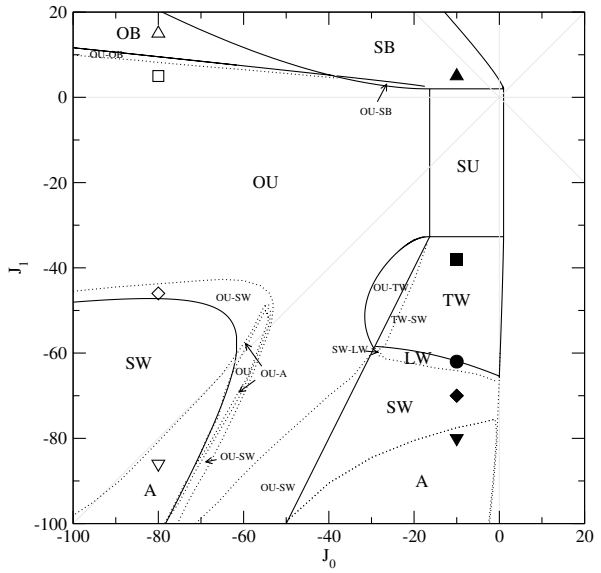

FIG. 1. Phase diagram of the rate model, Eq. (1), for $D = 0.1$. The states are: stationary uniform (SU), stationary bump (SB), oscillatory bump (OB), oscillatory uniform (OU), traveling waves (TW), standing waves (SW), lurching waves (LW), and aperiodic patterns (A). All solid lines have been determined analytically. Stability lines of other states (dotted lines) have been determined by numerical simulations. Regions of bistability are indicated by hyphens, e.g., OU-SW. Symbols refer to the patterns in Fig. 2. (For the case $D = 0$ see [6], Fig. 13.7.)

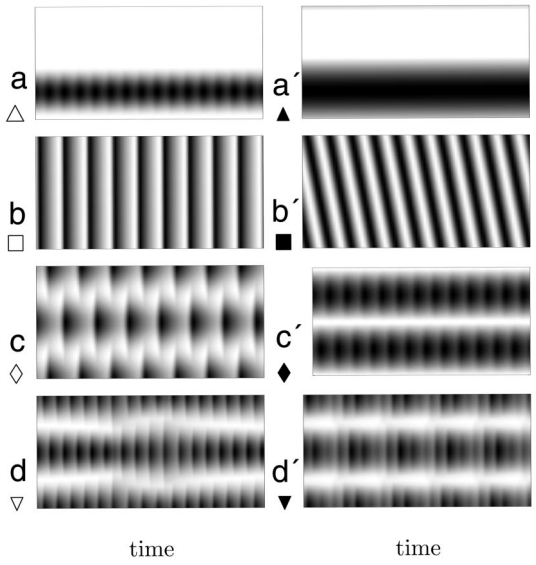

FIG. 2. Space-time plots of typical patterns of activity in the different regions of Fig. 1 shown over five units of time. Left-hand column from top to bottom: $J_0 = -80$ and $J_1 = 15, 5, -46, -86$ corresponds to OB, OU, SW, and A in Fig. 1. Right-hand column from top to bottom: $J_0 = -10$ and $J_1 = 5, -38, -70, -80$ corresponding to SB, TW, SW, and A. $D = 0.1$ and I is varied to maintain the mean firing rate at 0.1. Dark regions indicate higher levels of activity in gray scale. Symbols refer to the location of the patterns in the phase-diagram, Fig. 1.

[20]. Secondary instabilities of these states are investigated numerically as are the dynamical patterns to which the instabilities lead.

I. Stationary bumps.—As J_1 crosses the value of two from below a Turing instability of the SU state to a stationary bump of activity occurs, SB [Fig. 2(a′)]. The stability boundary of such bumps can be calculated analytically in Eq. (1), revealing two mechanisms of destabilization. For sufficiently strong local excitatory connectivity, a rate instability occurs ($m \to \infty$ as $t \to \infty$). For sufficiently strong inhibition, an oscillatory instability occurs. This instability may lead to the OU state, or to an oscillatory bump state, OB, for J_1 sufficiently large [Fig. 2(a)].

II. Oscillatory uniform.—Sufficiently strong global inhibition (i.e., J_0 negative enough), leads to a Hopf bifurcation to an OU state [Fig. 2(b)]. For small D, this Hopf bifurcation occurs for $J_0 \sim -\pi/(2D)$, and the frequency of the unstable mode at the bifurcation is $f \sim 1/(4D)$. The amplitude of the oscillatory instability grows until the input current crosses the threshold of the transfer function from above. The emerging limit cycle thus consists of a period, e.g., $0 < t < T_1$, in which the input current is negative and during which $m(x, t) \propto e^{-t}$. If the duration of this initial period is greater than the delay, $T_1 > D$, then in the subsequent time period, $T_1 < t < T_1 + D$, the solution will consist of a homogeneous exponential solution and a particular solution driven by the value of m in the preceding epoch. The complete limit cycle can be constructed by extending this reasoning to solve Eq. (1) for as many epochs as are required to cover the full period of oscillation, T. The latter is determined by the condition: $m(T) = m(0)$. Once the limit cycle $m_{lc}(t)$ has been found, its stability is determined by considering the ansatz $m(t) = m_{lc}(t) + \delta m_0(t) + \delta m_1(t)\cos(x)$, where δm_0 and δm_1 are small. The conditions $\delta m_i(T) = \beta_i \delta m_i(0)$ yield the Floquet multipliers β_i for $i = 0, 1$. If $D < T - T_1 < 2D$, then $\beta_0 = 1$ and

$$\beta_1 = e^{-T}\left(1 + \frac{J_1}{2}\mathrm{Re}^D + J_1^2\frac{(R-D)^2}{8}e^{2D}\right), \qquad (2)$$

where $R = T - T_1$. The homogeneous oscillations are stable if $|\beta_1| < 1$. For $\beta_1 = -1$, a period-doubling instability of the spatially heterogeneous mode occurs, leading to SW in which two distinct regions of the network oscillate out of phase with one another [Fig. 2(c)]. Numerical simulations show that further decreasing J_1 leads to additional instabilities to aperiodic patterns A [Fig. 2(d)]. A phase instability occurs for $\beta_1 = 1$. It can be shown that this condition is met, in particular, for $J_1 = 2J_0$, leading to SW. This condition is also met on an additional curve in the region $J_1 > 0$. The instability which occurs as one crosses this line from below leads either to an OB or a SB state, depending on J_0.

III. Traveling waves.—When J_1 is sufficiently negative ($J_1 \sim -\pi/D$ for small D), the SU state undergoes a bifurcation to TW. The profile of the wave can be derived,

yielding a relation for its velocity, $v = -\tan(vD)$. The TW state can destabilize along three curves in Fig. 1. If the global inhibition increases, an oscillatory instability to an OU state occurs. If local inhibition and long-range excitation are strengthened (i.e., decreasing J_1) an oscillatory instability of the waves leads to a lurching wave state [11,21], LW, in which the waves slow down and speed up periodically [20]. Simulations reveal that LW becomes unstable to SW as J_1 decreases [Fig. 2(c′)]. Further decreasing J_1 leads to additional bifurcations to more complex patterns with aperiodic dynamics, A [Fig. 2(d′)].

The stability boundaries of bumps, homogeneous oscillations, and waves indicate several regions of bistability (indicated by a hyphen in Fig. 1, e.g., OU-SW). Additional regions of bistability are found in numerical simulations bringing the total to eight for the phase diagram in Fig. 1.

In the limit $D \to 0$ all the bifurcation lines except the Turing instability line at $J_1 = 2$ and the rate instability lines go to negative infinity. Hence, only the SU and SB states survive in that limit. Beyond $D = 0.155$ the line defining the period-doubling instability from the OU to the SW state moves towards more negative values of J_0 and J_1. This line goes to infinity as D approaches 0.365, at which point the corresponding SW and A regions disappear [20].

The results presented thus far are for a threshold-linear transfer function and simplified connectivity. Simulations of Eq. (1) with other nonlinear transfer functions Φ reveal a qualitatively similar phase diagram in which all the dynamical regimes seen in Fig. 1 are present. Nonetheless, the nonlinearity of the transfer function determines the nature of the bifurcation and will thus alter the regions of bistability. A general, symmetric function J may introduce Turing and Turing-Hopf instabilities at higher wave number. While the simplicity of Eq. (1) allows for analysis, firing-rate models do not necessarily provide an accurate description of the dynamics of more realistic networks of spiking neurons (NSN). To what extent are the dynamics in Eq. (1) relevant for understanding the patterns of activity observed in the NSN? We consider a 1D network of conductance-based neurons with periodic boundary conditions, composed of two populations of N neurons: excitatory E and inhibitory I. All neurons are described by a Hodgkin-Huxley type model [22] with one somatic compartment. Na and K currents shape the action potentials. The probability of connection from a neuron in population $A(= E, I)$ to a neuron in population B is p_{BA}, where p depends on the distance r between them as $p_{BA} = p_0^{BA} + p_1^{BA}\cos(r)$. Synaptic currents are modeled as $I_{\text{syn},A} = -g_A s(t)(V - V_A)$, $A \in E, I$, where V is the voltage of the post-synaptic neuron, V_A is the reversal potential of the synapse (0 mV for $A = E$ and -80 mV for $A = I$), g_A is the maximum conductance change, and $s(t)$ is a variable which, given a presynaptic spike at time $t^* - \delta$, takes the form $s(t) = \frac{1}{\tau_1 - \tau_2}(e^{-(t-t^*)/\tau_1} - e^{-(t-t^*)/\tau_2})$, where δ is the delay and τ_1 and τ_2 are the rise and decay times. Finally, each neuron receives external, excitatory synaptic input as a Poisson process with a rate ν_{ext}, modeled as the synaptic currents above with a maximum conductance change of g_{ext}. To compare the dynamical patterns found in the NSN and their dependence on the parameters with those of the firing-rate model we choose $p_{IE} = p_{EE} = p_E$, $p_{EI} = p_{II} = p_I$ and identical synaptic time constants for excitatory and inhibitory connections ($\tau_1 = 1$ ms and $\tau_2 = 3$ ms). This creates an effective one-population network with an effective coupling similar to that of the rate model. Figure 3 shows eight typical firing patterns in the NSN. The figures have been arranged to allow comparison with those in Fig. 2. The patterns show good qualitative agreement, and were obtained by altering the network parameters in a way analogous to those changes made in the rate model to produce Fig. 2. The only state that could not be seen in a robust way in the NSN was the TW. However, transient dynamics in the region where stable SW are found show short-lived TW which eventually lose out to an oscillatory mode, causing the waves to break up into distinct oscillating subgroups of neurons; see [20]. From the eight regions of bistability displayed by Eq. (1), at least one (OU-SW) is

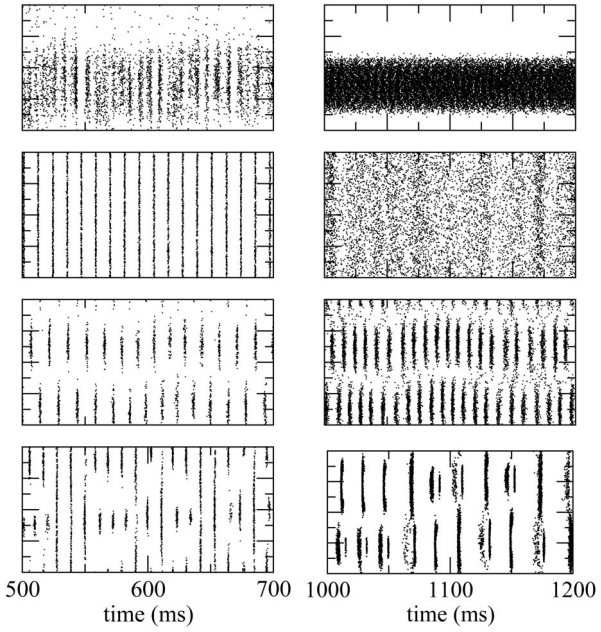

FIG. 3. Typical firing patterns in a NSN. See text for details. Compare with Fig. 2. The network consists of two populations of 2000 neurons each. Left-hand column from top to bottom: a localized bump with oscillations, homogeneous oscillations, a period-doubled state of oscillating bumps, and a chaotic state. Parameters: $p_0^E = 0.2, 0, 0, 0$, $p_0^I = 0.2, 0.5, 0.5, 0.5$, $p_1^E = 0.1, 0, 0, 0$, $p_1^I = 0, 0, 0.2, 0.5$, $g_E = 0.1, 0, 0, 0$, $g_I = 0.28, 0.1, 0.1, 0.1$, $\nu_{\text{ext}} = 2000, 15\,000, 15\,000, 15\,000$, and $g_{\text{ext}} = 0.01$. $\delta = 0$ ms. Right-hand column from top to bottom: a steady and localized bump, the stationary uniform state, oscillating bumps and a chaotic state. Parameters: $p_0^E = 0.2$, $p_0^I = 0.2$, $p_1^E = 0.2, 0, 0, 0$, (top to bottom) $p_1^I = 0, 0, 0.2, 0.2$, $g_E = 0.01, 0.01, 0.01, 0.1$, $g_I = 0.028, 0.028, 0.028, 0.28$, $\nu_{\text{ext}} = 500, 500, 5000, 500$, and $g_{\text{ext}} = 0.01, 0.01, 0.001, 0.01$. $\delta = 0, 0, 0, 2.0$ ms.

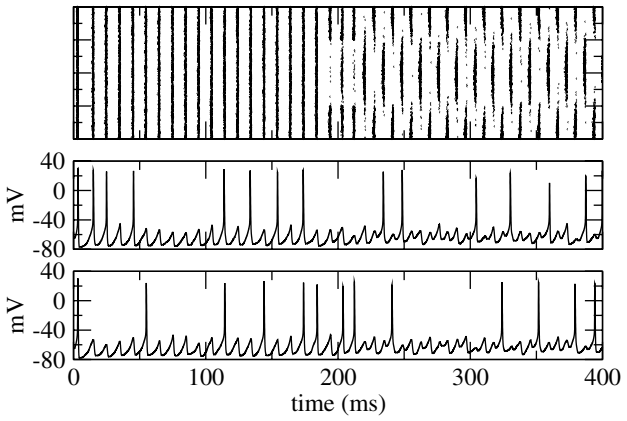

FIG. 4. Bistability between uniform oscillations and an oscillating bump state in a purely inhibitory network. A 30 ms inhibitory pulse is applied to neurons 500 through 1500 around time 200. This induces a state in which two groups of neurons oscillate out of phase with one another; cf. voltage trace of neuron 1000 (middle) and neuron 1 (bottom). Parameters are $p_0^I = 0.4$, $p_1^I = 0.2$, $g_I = 0.1$, $\nu_{\text{ext}} = 4500$, $g_{\text{ext}} = 0.033$, and $\delta = 0.5$ ms.

also present in the NSN in an analogous parameter regime; see Fig. 4.

In summary, we have shown that the presence of delays leads to a wide variety of spatio-temporal patterns and the existence of various regions of multistability. For sufficiently strong spatial modulation of inhibition, a period-doubling bifurcation from homogeneous oscillations to SW occurs. This SW state is achievable in purely inhibitory networks. Interestingly, a similar bifurcation occurs in spatially extended systems near a homoclinic orbit [23]. Further bifurcations of the SW state to aperiodic and chaotic dynamics occur as the spatial modulation becomes stronger. Delays are furthermore responsible for the emergence of waves given neural interactions which are locally inhibitory and excitatory at longer distances (region $0 > J_0 > J_1$ in Fig. 1). Introducing a distribution of delays in Eq. (1) does not, in general, alter our results qualitatively ([20]). The dynamical states displayed by Eq. (1) are found in the NSN also in the *absence* of synaptic delays ($\delta = 0$) (Fig. 3) and even if $\tau_1 = 0$ (not shown here). This is because action potential initiation dynamics in Hodgkin-Huxley-type neurons introduce an *effective* delay [13], which is captured in the reduced model Eq. (1) if $D \neq 0$. Hence, in the NSN, explicit delays are not required to reproduce the dynamical regimes seen in Fig. 1. Localized waves and bumps have been studied in rate models with delays that depend on the distance between neurons, e.g., [24]. An extension of this work with such delays is in progress.

Finally, we showed that mutual inhibition with spatially decaying connectivity, if sufficiently modulated in space, can lead to bistability. We suggest that such states could play a role in memory storage. This would be in contrast to traditional scenarios for short-term memory in which bistability is due to recurrent excitation.

We thank C. Meunier and B. Gutkin for helpful comments. A. R. was supported by NSF Grant No. 0302085.

[1] V. B. Mountcastle, Brain **120**, 701 (1997).
[2] G. González-Burgos, G. Barrionuevo, and D. A. Lewis, Cereb. Cortex **10**, 82 (2000).
[3] K. A. C. Martin, Quarterly Journal of Experimental Physiology: An International Journal of the Physiological Society **73**, 637 (1988).
[4] M. Tsodyks, T. Kenet, A. Grinvald, and A. Arieli, Science **286**, 1943 (1999).
[5] R. Ben-Yishai, R. Lev Bar-Or, and H. Sompolinsky, Proc. Natl. Acad. Sci. U.S.A. **92**, 3844 (1995).
[6] D. Hansel and H. Sompolinsky, in *Methods in Neuronal Modeling*, edited by C. Koch and I. Segev (MIT Press, Cambridge, MA, 1998), 2nd ed..
[7] D. C. Somers, S. B. Nelson, and M. Sur, J. Neurosci. **15**, 5448 (1995).
[8] A. Compte, N. Brunel, P. S. Goldman-Rakic, and X.-J. Wang, Cereb. Cortex **10**, 910 (2000).
[9] B. S. Gutkin, C. R. Laing, C. L. Colby, C. C. Chow, and G. B. Ermentrout, J. Comput. Neurosci. **11**, 121 (2001).
[10] R. Ben-Yishai, D. Hansel, and H. Sompolinsky, J. Comput. Neurosci. **4**, 57 (1997).
[11] D. Golomb and G. B. Ermentrout, Proc. Natl. Acad. Sci. U.S.A. **96**, 13480 (1999).
[12] H. Markram, J. Lubke, M. Frotscher, A. Roth, and B. Sakmann, J. Physiol. (London) **500**, 409 (1997).
[13] N. Fourcaud-Trocmé, D. Hansel, C. van Vreeswijk, and N. Brunel, J. Neurosci. **23**, 11628 (2003).
[14] N. Brunel and V. Hakim, Neural Comput. **11**, 1621 (1999).
[15] N. Brunel and X.-J. Wang, J. Neurophysiol. **90**, 415 (2003).
[16] H. R. Wilson and J. D. Cowan, Kybernetik **13**, 55 (1973).
[17] S. Amari, Biol. Cybern. **27**, 77 (1977).
[18] G. B. Ermentrout, Rep. Prog. Phys. **61**, 353 (1998).
[19] P. C. Bressloff, in *Methods and Models in Neurophysics, Les Houches 2003 Session LXXX*, edited by C. Chow, B. Gutkin, D. Hansel, C. Meunier, and J. Dalibard (Elsevier, Amsterdam, 2003).
[20] See EPAPS Document No. E-PRLTAO-94-061525 for the analytical framework and calculations for the stability analysis of nonlinear firing patterns (stationary bumps, oscillatory uniform state, and traveling waves) in the firing-rate equation with threshold-linear transfer function and cosine coupling. Phase diagrams for different values of the delay (D). A direct link to this document may be found in the online article's HTML reference section. The document may also be reached via the EPAPS homepage (http://www.aip.org/pubservs/epaps.html) or from ftp.aip.org in the directory /epaps/. See the EPAPS homepage for more information.
[21] D. Golomb, X. J. Wang, and J. Rinzel, J. Neurophysiol. **75**, 750 (1996).
[22] X.-J. Wang and G. Buzsáki, J. Neurosci. **16**, 6402 (1996).
[23] M. Argentina, P. Coullet, and F. Risler, Phys. Rev. Lett. **86**, 807 (2001).
[24] S. Coombes, G. J. Lord, and M. R. Owen, Physica D (Amsterdam) **178**, 219 (2003).